Nuclear Materials and Energy 24 (2020) 100770

Contents lists available at ScienceDirect

Nuclear Materials and Energy

journal homepage: www.elsevier.com/locate/nme

Microstructure, oxidation behaviour and thermal shock resistance of self-passivating W-Cr-Y-Zr alloys

Elisa Sal[a,b], Carmen García-Rosales[a,b,*], Karsten Schlueter[c,d], Katja Hunger[c], Mauricio Gago[e], Marius Wirtz[e], Aida Calvo[a,b], Iñigo Andueza[a], Rudolf Neu[c,d], Gerald Pintsuk[e]

[a] Ceit Technology Center, 20018 San Sebastian, Spain
[b] Universidad de Navarra, Tecnun, 20018 San Sebastian, Spain
[c] Max-Planck-Institut für Plasmaphysik, 85748 Garching, Germany
[d] Technische Universität München, 85748 Garching, Germany
[e] Forchungszentrum Jülich GmbH, Institute of Energy and Climate Research, 52425 Jülich, Germany

ARTICLE INFO

Keywords:
Self-passivating tungsten alloy
Oxidation resistance
Thermal shock resistance
Plasma-facing materials

ABSTRACT

Self-passivating tungsten based alloys for the first wall armor of future fusion reactors are expected to provide an important safety advantage compare to pure tungsten in case of a loss-of-coolant accident with simultaneous air ingress, due to the formation of a stable protective scale at high temperatures in presence of oxygen preventing the formation of volatile and radioactive WO_3. In this work, Zr is added to self-passivating W-10Cr-0.5Y alloy, manufactured by mechanical alloying and HIP, in view of improving its mechanical strength and thus, its thermal shock resistance. The as-HIPed W-10Cr-0.5Y-0.5Zr exhibits a nanocrystalline microstructure with the presence of an extremely fine nanoparticle dispersion. After heat treatment at 1555 °C for 1.5 h, the grain size growths from less than 100 nm to 620 nm and nanoparticles are present both at the grain boundaries and inside the grains. Oxidation tests at 1000 °C revealed that the alloy with Zr exhibits also a strong oxidation reduction compared to pure W. The long-term oxidation rate is similar to that of the alloy without Zr. Under thermal shock loading simulating 1000 ELM-like pulses at the divertor, the heat treated Zr-containing alloy did not present any damage.

1. Introduction

Tungsten is currently the main candidate armor material for plasma facing components of future fusion reactors such as DEMO. However, the use of pure tungsten implies a potential risk in terms of safety. In case of a loss-of-coolant accident with simultaneous air ingress, a temperature increase of the in-vessel components above 1000 °C is expected due to the decay heat, remaining at high temperature for tens of days [1]. Under this situation, the use of pure tungsten would result in full oxidation of the armor because of its high oxidation rate at high temperatures, causing the formation of volatile and radioactive tungsten oxides that could be released to the atmosphere [2,3]. A possible way to avoid this safety issue is the addition of oxide-forming alloying elements to pure tungsten, resulting in the formation of a self-passivating layer at high temperatures in presence of oxygen. Besides high affinity to oxygen to form stable oxides with high melting temperature, the alloying elements have to form adherent oxide scales and to exhibit low volume increase of the oxides and low activation by neutron irradiation [4–7]. During normal operation, the surface of the self-passivating alloy will consist of pure tungsten due to preferential sputtering of the alloying elements by plasma ions. The material of the blanket first wall (FW) requires a high thermal shock resistance to withstand, not only the expected thermal load during normal plasma operation, but also transient thermal loads like so-called edge localized modes (ELMs), during which a large amount of energy is loaded on the plasma facing materials in a very short time [8].

In previous works [9], it has been shown that bulk alloys of the system W-Cr-Y, manufactured by mechanical alloying (MA) and subsequent hot isostatic pressing (HIP) with an additional heat treatment at 1550 °C present acceptable mechanical properties and good thermal shock resistance. Furthermore, these self-passivating alloys result in a reduction of the oxidation rate by 3–4 orders of magnitude at temperatures up to 1000 °C compared to pure tungsten [10–12]. In other investigations [13–16] Zr was added to tungsten in view of improving its mechanical properties by strengthening the grain boundaries (GBs) with a nanodispersion of ZrO_2. In this way, Zr "cleans" the GBs from

* Corresponding author at: Ceit-IK4 Technology Center, 20018 San Sebastian, Spain.
E-mail address: cgrosales@ceit.es (C. García-Rosales).

https://doi.org/10.1016/j.nme.2020.100770
Received 31 January 2020; Received in revised form 4 June 2020; Accepted 23 June 2020
Available online 29 June 2020

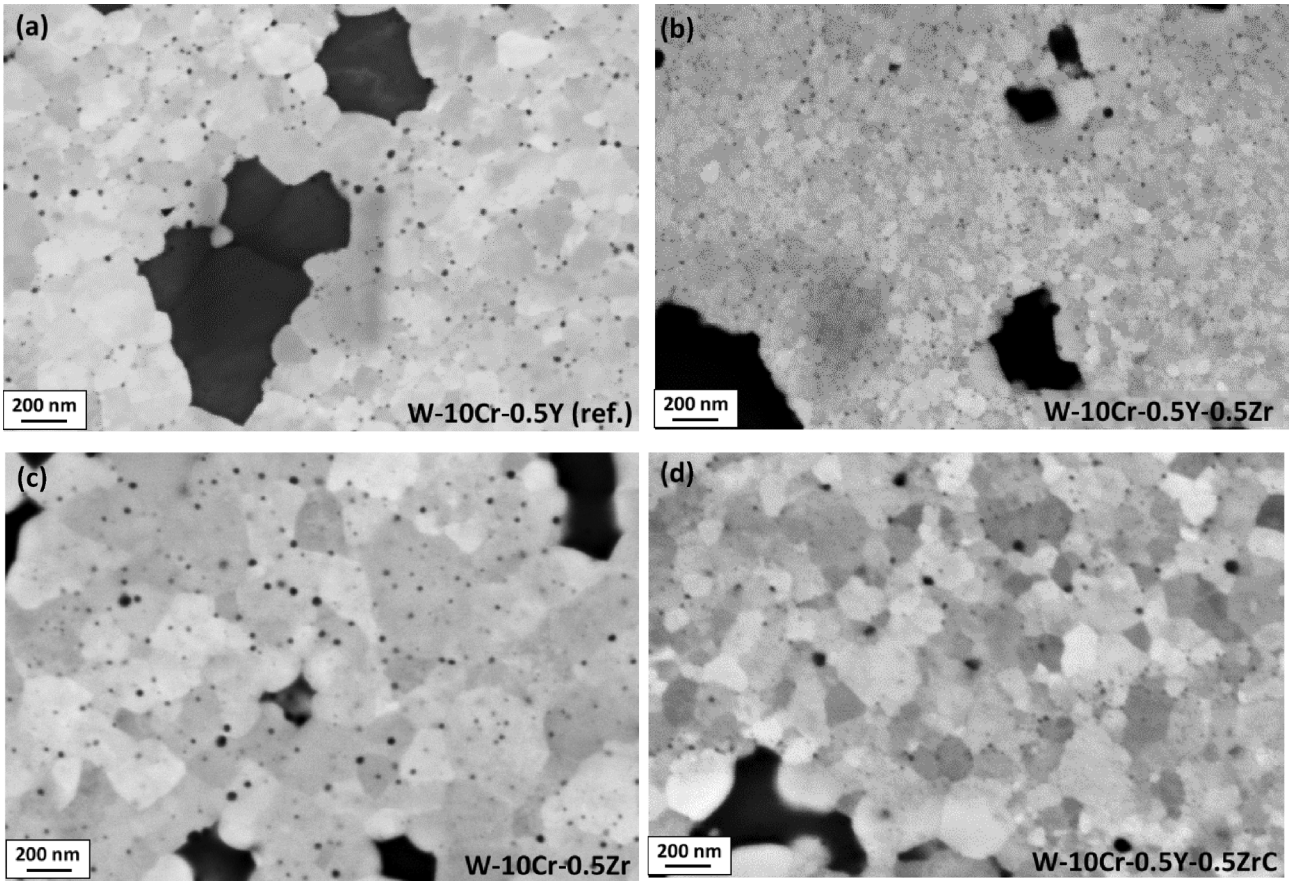

Fig. 1. FEG-SEM images after HIP of (a) W-10Cr-0.5Y, (b) W-10Cr-0.5Y-0.5Zr, (c) W–10Cr–0.5Zr and (d) W-10Cr-0.5Y-0.5ZrC alloys.

oxygen. Besides, Z.M. Xie et al [17] reported the existence of a coherent interface between tungsten and ZrC dispersoids contributing to lock GB sliding, thus increasing their cohesion. This mechanism allows improving the strength and ductility of tungsten. In this context, adding elemental Zr to W-Cr-Y alloys would lead to its combination with undesirable interstitial oxygen and carbon introduced by MA. On the other hand, Zr may also contribute to improve the oxidation resistance, as recently reported for thin film alloys of the system W-Cr-Zr [18], with a comparable passivating behaviour to thin films of W-Cr-Y [11]. The addition of Zr in form of ZrC may also be of interest to produce a strengthening of the GBs.

The aim of this research is to develop Zr-containing self-passivating alloys with good oxidation resistance and high thermal shock resistance improving the results obtained in previous work with the W-10Cr-0.5Y system. In the present work, three different systems with compositions W–10Cr-0.5Zr, W-10Cr-0.5Y-0.5ZrC and W–10Cr–0.5Y–0.5Zr are manufactured by MA and HIP. Screening oxidation tests are performed to select the best alloy regarding oxidation and thus, the best way for introducing Zr (in elemental form or as a carbide). The selected Zr-containing alloy is subjected to oxidation and thermal shock tests. The results of these tests as well as microstructural analysis are presented and compared to the W-10Cr-0.5Y alloy of previous investigations.

2. Experimental

Elemental powders of pure W (99.95%, 15–30 μm), Cr (99.95%, 74 μm), Y (99.9% 40–50 μm) and Zr (99%, 4.5–6.5 μm), as well as ZrC (99.5%, 44 μm) were used to produce samples of four different systems: W-Cr-Y (considered as reference alloy), W–Cr-Zr, W-Cr-ZrC and W-Cr-Y-Zr. The Cr and Y contents were 10 wt% and 0.5%, respectively, for all systems, and the ZrC or Zr contents 0.5 wt%. These powders were mechanically alloyed under Ar atmosphere in a planetary ball mill using WC balls and jars. The MA parameters were those considered as optimum for the W-Cr-Y system in previous work [19]. Metallic capsules with the alloyed powder were evacuated, degassed, sealed and HIPed at 1250 °C for 2 h at 140 MPa. A HT at 1555 °C for 1.5 h under hydrogen atmosphere was performed on HIPed samples to obtain a single-phase material. The density of the samples was determined by the Archimedes method and from weight and volume. The theoretical density was calculated by the rule of mixtures. Powders and bulk samples were characterized by field emission scanning electron microscopy (FE-SEM) and energy dispersive X-ray spectroscopy (EDS) as well as by X-ray diffraction (XRD). The average grain size of materials after HIP or HT was determined by quantitative metallography. The oxygen and nitrogen contents of powders bulk samples were measured with a LECO TC-400, using the inert gas fusion method (ASTM E1569), and the carbon content by the combustion method with a LECO CS-200 (ASTM E1019).

In a first step, samples of each system were exposed to isothermal oxidation in a furnace under atmospheric air at 1000 °C for 24 h as a kind of screening to select the best system regarding oxidation. Then, the selected system (W-Cr-Y-Zr) was tested under isothermal oxidation at 1000 °C up to 60 h by thermogravimetric analysis (TGA) using a mixture of 80 vol% Ar and 20 vol% O_2 at atmospheric pressure with preheating and cooling down both in Ar. The mass gain of the samples due to oxide formation was measured by a thermobalance with a sensitivity of 0.025 μg. The procedure is described in detail in [20]. Oxidation tests simulating accident-like conditions were also conducted. These tests consisted of a preheating in Ar up to 600 °C followed by oxidation in a mixture of 80 vol% Ar and 20 vol% O_2 at linear increasing temperature from 600 to 1000 °C during about 17 h, two isothermal oxidation steps in Ar/20% O_2 at 1000 °C for 1 h, each of

them followed by isothermal steps in Ar (without O_2) at 1000 °C for 1 h, and cooling down in Ar. Surfaces and cross sections of oxidized samples were analyzed by FE-SEM, EDS and focused ion beam (FIB).

Thermal shock tests were performed at the linear plasma device PSI-2 on samples of dimensions 10 × 10 × 5 mm^3. The procedure is described in detail in [21]. Samples were exposed at a base temperature of 400 °C to loads consisting of 100 and 1000 pulses with power densities of 0.19 GW/m^2 (only 1000 pulses) and 0.38 GW/m^2 for 1 ms to simulate the conditions expected at the divertor under ELMS. Samples were also subjected to one disruption-like load of 1.6 GW/m^2 and 2 ms duration to simulate a disruption event. After exposure to both ELMs- and disruption loads, the surface and cross section of the samples were analyzed by optical microscopy.

3. Results and discussion

3.1. Screening of Zr-containing alloys

Mechanically alloyed powders of compositions W–10Cr–0.5Y, W-10Cr-0.5Zr, W–10Cr–0.5Y-0.5Zr and W-10Cr-0.5Y-0.5ZrC were encapsulated, sealed and HIPed at 1250 °C for 2 h. The relative density was in all cases practically 100%.

3.1.1. Microstructure

In Fig. 1 the microstructure of the as-HIPed W-10Cr-0.5Y-0.5Zr, W-10Cr-0.5Zr and W-10Cr-0.5Y-0.5ZrC is shown and compared to the one of the reference W-10Cr-0.5Y alloy, whose grain size is 110 ± 4 nm [9]. When comparing the microstructure of the W-10Cr-0.5Y-0.5Zr alloy (Fig. 1(b)) with the one of the reference alloy W-10Cr-0.5Y (Fig. 1(a)) it can be clearly seen that the addition of elemental Zr to W-10Cr-0.5Y results in a significant reduction of particle size: matrix grains with average size well below 100 nm and a higher density of significantly smaller nanoparticles (NPs) are appreciated in the W-10Cr-0.5Y-0.5Zr alloy. This is an indication that both Y and Zr are very efficient inhibitors of grain growth. The Y-rich and Zr-rich NPs cannot be distinguished, and TEM analysis would be required to identify them and to determine whether Zr is present in form of ZrO_2 or also as ZrC. It is assumed that most of the elemental Zr will form ZrO_2 due to its much more negative Gibb's energy of formation compared to ZrC (−1092 kJ/mol at RT for the oxide compared to –96 kJ/mol for the carbide [22]). Nevertheless, it is likely that, once the reservoir of oxygen introduced during MA is consumed for the oxide formation, the remaining Zr may be combined with the residual carbon also introduced during MA to form ZrC.

If only elemental Zr (without Y) is introduced (comparison of W-10Cr-0.5Zr, Fig. 1(c), with the reference W-10Cr-0.5Y alloy Fig. 1(a)), then the grain size clearly increases, indicating that Y is a more efficient grain growth inhibitor than Zr. The Zr-containing NPs are significantly larger than in the previous case and are not located at the GBs, as in the W-10Cr-0.5Y-0.5Zr and W-10Cr-0.5Y alloys, but inside the matrix grains.

If ZrC is added to W-10Cr-0.5Y (comparison of W-10Cr-0.5Y-0.5ZrC Fig. 1(d) with the reference W-10Cr-0.5Y alloy), a slight decrease of particle size is observed. The NP are smaller than those observed in the alloy without ZrC and they seem to be located both at the GB and inside the grains. According to this, one can assert that ZrC further contributes to inhibit grain growth.

If Zr is added to W-10Cr-0.5Y in form of ZrC instead of elemental Zr (comparison of W-10Cr-0.5Y-0.5Zr (b) and W-10Cr-0.5Y-0.5ZrC (d) alloys), it can be clearly observed that the inhibition of grain growth is more efficient with the addition of elemental Zr than by adding it as ZrC.

Summarizing all observations, we can conclude that

- The addition of Zr and Y leads to a very effective inhibition of grain growth
- The addition of only Zr is not so an efficient grain growth inhibitor, since the NPs are larger and located mainly inside grains
- Elemental Zr is a more efficient grain growth inhibitor than ZrC

According to these results, the W-10Cr-0.5Y-0.5Zr is the best system from the point of view of the microstructure.

3.1.2. Screening oxidation tests

A screening isothermal oxidation test was performed at 1000 °C for 24 h in a furnace under atmospheric air in order to have a first impression of the oxidation behavior of the three Zr-containing systems and to compare them to the reference alloy. The surfaces of the oxidized samples and the formed scales were analyzed by FEG-SEM and EDS (analysis not included here). It is observed that the thickness of the oxide scale is similar for the alloys with and without Zr, indicating that the addition of only Zr (elemental) lead also to a strong reduction of oxidation, even though the combination of Y + Zr seems to lead to a better passivating effect. It was also observed that Zr is always associated to the thin Cr_2O_3 passivating surface layer formed at the reference W-10Cr-0.5Y and described in previous works [9,10,23]. Besides, in the sample containing ZrC (W-10Cr-0.5Y-0.5ZrC), a slight cobalt contamination originated from the WC (containing a small amount of Co as binder) vials and balls during MA is detected at the surface, which was not noticed at the bulk due to its low concentration. This contamination could be due to the abrasive nature of ZrC. It seems that Co diffuse preferentially to the surface during oxidation so that it can be just detected by EDS. This Co contamination is also present at the sample with only Zr addition (without Y, i.e.W-10Cr-0.5Zr) but to a less extent, probably because of the lower hardness of ZrO_2 formed during MA compared to that of ZrC [24]. No contamination was found in the W-10Cr-0.5Y-0.5Zr alloy. Such a Co contamination was never detected in previous samples of the W-Cr-Y system. The reason can be the lower hardness (and thus less abrasive effect) of Y_2O_3 compared to that of ZrO_2, since in the W-10Cr-0.5Y-0.5Zr alloy Y combines first with oxygen and then with Zr due to the higher affinity of Y to oxygen [22].

Summarizing the previous screening oxidation results, we can conclude that

- -There are no relevant differences among samples with Zr addition and compared to the reference alloy with regard to their oxidation behavior.
- -Zr is always associated to the thin Cr_2O_3 layer and seems to slightly reinforce its passivating effect.
- -In the alloys with only Zr (W-10Cr-0.5Zr) and with Zr in form of ZrC (W-10Cr-0.5Y-0.5ZrC) there is a slight Co contamination from vials/balls from MA. This is not the case for the W-10Cr-0.5Y-0.5Zr alloy.

According to these results, the W-10Cr-0.5Y-0.5Zr is also the best system from the point of view of Co-contamination from vials and balls during MA.

3.2. Characterization and testing of W-10Cr-0.5Y-0.5Zr alloy

New samples of the selected Zr-containing alloy, W-10Cr-0.5Y-0.5Zr, and of the reference W-10Cr-0.5Y alloy were manufactured. After HIPing the relative densities of the materials were above 99% in all cases. The contents of interstitial elements after MA for both alloys are listed in Table 1. These amounts remain unchanged after HIPing. The amount of oxygen in the Zr-containing alloy is such that, if only Y and Zr combine with oxygen, the whole Y content and part of the Zr content will exhaust the whole oxygen content, cleaning the GBs from oxygen (Y_2O_3 has a lower Gibbs energy than ZrO_2 and will react first). Besides, the amount of residual Zr content is approximately the one required to react with the whole carbon present in the alloy to form ZrC.

A HT was performed after HIP at 1555 °C in order to dissolve the Cr-

Table 1
Impurity contents after MA in the reference and Zr-containing alloys.

	Impurities (ppm)		
	O	N	C
W-10Cr-0.5Y (ref.)	1100–1400	100 – 200	250–400
W-10Cr-0.5Y-0.5Zr	2100–2300	70–100	300–400

rich phase obtaining a single-phase material. After HT, a slight density reduction of about 1.5% is observed for the reference alloy, while for de Zr-containing alloy this reduction is about 0.2%, i.e. almost negligible. This density decrease was found to be caused by the presence of unalloyed Cr-particles, to which porosity is always associated. According to [25], Cr has a much higher amount of vacancies than W, and Cr atoms exhibit a significantly higher mobility than W atoms, so that the latter can be regarded as immobile compared to Cr atoms. For this reason, Cr atoms cannot diffuse into W (negligible mobility, no vacancies) while W atoms can jump into vacancies of Cr. W atoms diffuse towards unalloyed Cr particles and the GBs will move towards the Cr-rich side, while Cr atoms diffuses much faster out of the unalloyed Cr grain though the GBs. I.e., there is a Kirkendall effect generating porosity inside the unalloyed Cr particles. The fact that in the Zr-alloy, the density reduction is significantly lower in spite of the presence of some unavoidable unalloyed Cr particles may indicate that Cr diffusion is hindered by the presence of a high density number of very small NPs.

3.2.1. Microstructure after HT

The microstructure of the W-10Cr-0.5Y-0.5Zr and reference alloy after HIP and subsequent HT at 1555 °C is shown in Fig. 2. It consists of a single (αW,Cr) phase with equiaxed grains of an average size of 813 ± 4 nm for the reference alloy and 620 ± 12 nm for the alloy with Zr. Significant grain growth after HT is thus observed, but in the case of Zr-containing alloy, it is less remarkable. However, the main difference between the alloys with and without Zr after HT is the presence of much smaller NPs in the alloy containing Zr, located not only at the GBs but also inside the grains. TEM analysis is required to identify the composition of the NPs. However, since the amount of oxygen is not enough to combine with the whole amount of Y and Zr present in the alloy, it is assumed, as mentioned above, that part of the Zr combines with the C introduced during MA to form ZrC. This has to be confirmed by TEM in future work. In any case, it can be assumed that the presence of such a fine NP dispersion will positively influence the mechanical properties.

3.2.2. Oxidation tests

Isothermal oxidation tests at 1000 °C for 60 h as well as tests simulating accident-like conditions up to 1000 °C were performed on the as-HIPed and HIP + HT W–10Cr–0.5Y–0.5Zr alloy and compared to the reference alloy (also as-HIPed and HIP + HTed). In Fig. 3, the mass gain per unit area of each alloy during isothermal oxidation is shown. The orange line represents the mass gain of pure W, whose oxidation rate is 3–4 orders of magnitude higher than self-passivating W-Cr-Y alloys [9]. The overall mass gains for the reference and Zr-containing alloys are quite similar, being those for the Zr-containing alloy lower after high exposure times. The oxidation kinetics is parabolic for the initial phase, becoming linear for longer exposure times with similar linear oxidation rates for the reference and Zr-containing alloy (same slope of the linear part). Besides, there is no significant difference between the isothermal behavior of the as-HIPed and the HIP + HTed Zr–containing alloys. In the case of the reference alloy, the curve of the HTed sample coincides with the one of the Zr-containing alloys at the initial parabolic phase while after about 25 h there is a slow transition to higher mass gains, probably associated with a deterioration and subsequent recovery of the protective Cr_2O_3 scale.

The results of oxidation tests simulating accident-like conditions up to 1000 °C are presented in Fig. 4. The Zr-containing alloys exhibit the lowest mass gain, being the as-HIPed alloy slightly better than the HTed alloy even though the difference is within the drift of the thermo-balance. In the isothermal steps with oxygen, especially in the second one, the oxidation kinetics is parabolic with a higher rate for the reference alloy, in agreement with the isothermal oxidation tests shown above. Besides, during the isothermal segments without oxygen there is a slight linear mass gain with higher slope in the first step and almost negligible slope for the reference alloy during the second step. The mass gain during these steps without oxygen can be due to the residual oxygen present in Ar, or to oxygen solved or trapped in the oxide layer. In any case, it indicates that tungsten oxide sublimation leading to mass loss does not have an important influence on the oxidation behavior.

The cross-sections of the HTed Zr-containing and reference alloy after isothermal oxidation are presented in Fig. 5. Three different layers can be distinguished: a thin Cr_2O_3 layer, a thin Cr_2WO_6 scale just below followed by a thicker WO_3 scale, in agreement with previous works [9,24,12]. Oxygen diffusion through the whole oxide scale towards the alloy results in the formation of Cr_2O_3 at the GBs of the (αW,Cr) matrix. In both alloys, the total oxidized scale thickness after isothermal oxidation at 1000 °C for 60 h is approximately 17 μm, which means that Zr does not provide relevant improvement (nor worsening) compared to the reference alloy concerning oxidation.

3.2.3. Thermal shock tests

The as-HIPed and the HIP + HTed Zr-containing alloys were exposed at the PSI-2 facility to 1000 heat pulses of 0.19 GW/m^2 for 1 ms at 400 °C and subsequently to 100 and 1000 pulses of 0.38 GW/m^2 simulating ELM-like loading in the divertor. The sample surfaces after 1000 pulses of 0.38 GW/m^2 are shown in Fig. 6. A fine crack network

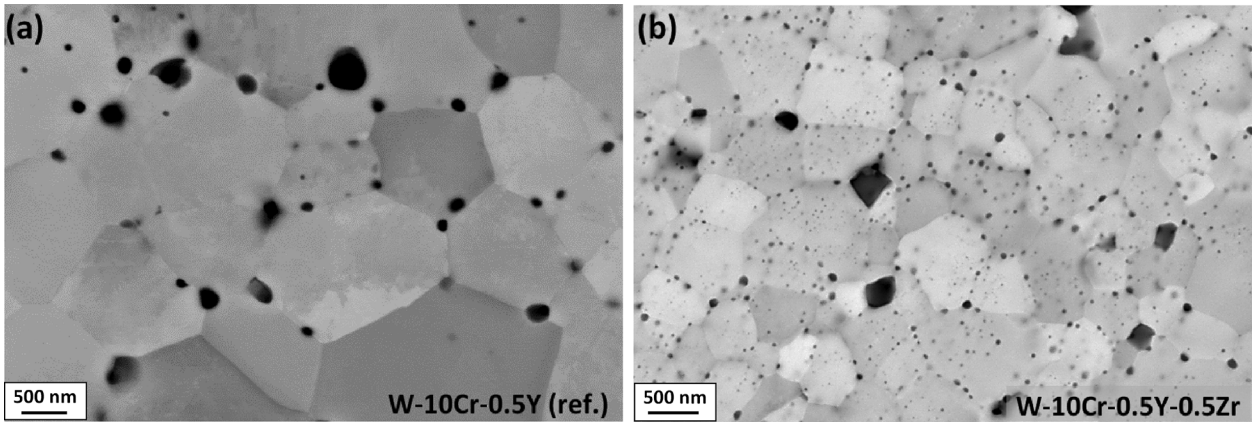

Fig. 2. Microstructure after HIP + HT of (a) W-10Cr-0.5Y and (b) W–10Cr–0.5Y–0.5Zr.

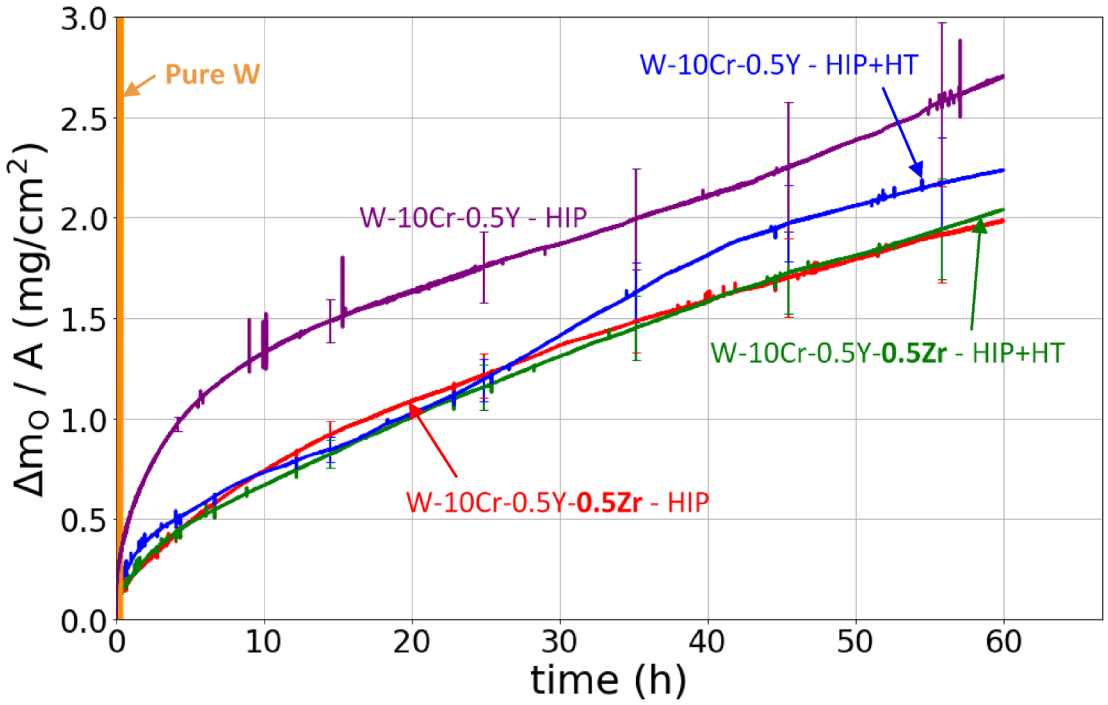

Fig. 3. Mass gain per unit area during isothermal oxidation at 1000 °C for 60 h of as-HIPed and HIP + HTed W–10Cr-0.5Y-0.5Zr and reference alloy. The error bars corresponds to the drift of the thermo-balance provided by the TGA manufacturer.

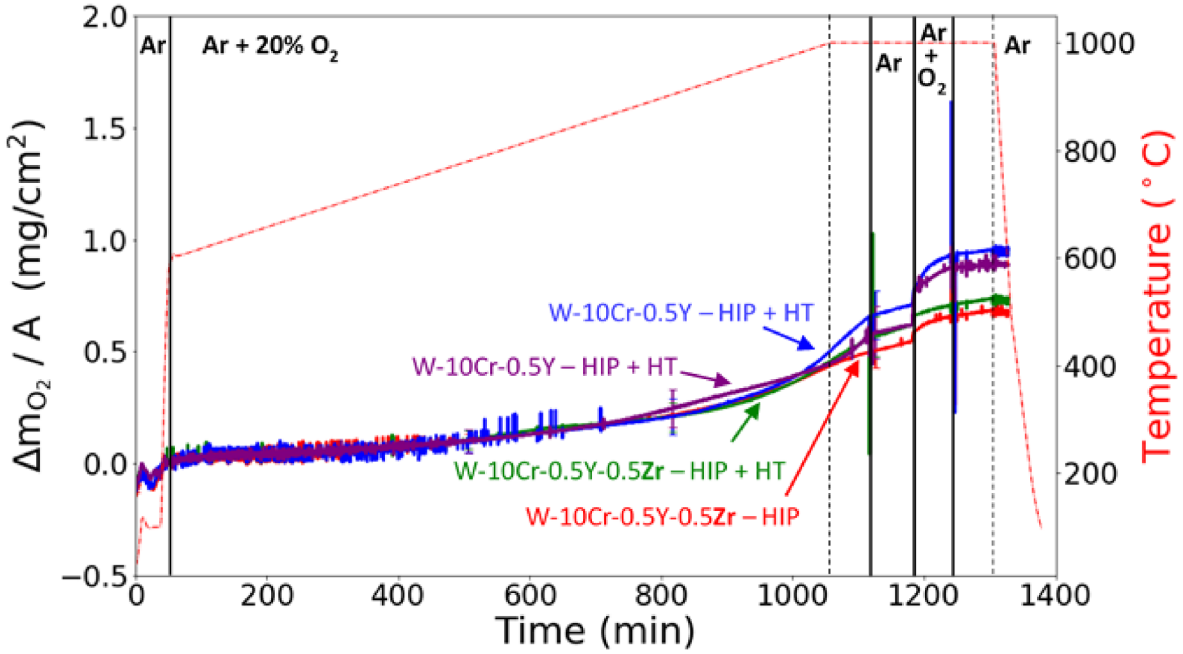

Fig. 4. Mass increase per unit area during oxidation under accident-like conditions on as-HIPed and HIP + HTed Zr-containing alloy and reference alloy. After preheating in pure Ar up to 600 °C, Ar/20% O_2 is introduced and the temperature is increased linearly from 600 to 1000 °C, followed by 1 h isothermal oxidation in air at 1000 °C, an isothermal step in pure Ar for 1 h, repetition of the two isothermal steps and cooling down in Ar.

without chipping is observed in the as-HIPed Zr-containing alloy (Fig. 6 (a)) while no damage is detected in the HTed alloy (Fig. 6 (b)). For comparison, the surface of the reference alloy (as-HIPed and HTed at 1550 °C) after the same loading at the JUDITH-1 electron beam facility is also shown in Fig. 6 (c,d), where chipping was detected in the as-HIPed sample, whereas in the sample with additional HT a crack network without chipping was observed [9]. Wirtz et al. [26] exposed the pure tungsten reference material IGP W to the same loading conditions at the JUDITH-1 facility, resulting in roughening and a crack network with cracks lengths of a few 100 µm.

In Fig. 7, the cross sections of these crack networks are shown. These results confirm those observed on the surface where the HTed alloy with Zr presents the best thermal shock resistance with no cracks. Assuming that the thermal conductivity of the Zr-containing alloy is similar to the one of the reference alloy, the improvement of the thermal shock behavior can be attributed to the presence of the previously described (Fig. 2(b)) fine NP dispersion of Y- and Zr-rich oxides at the GB and probably ZrC at the GB and inside the grains, acting as

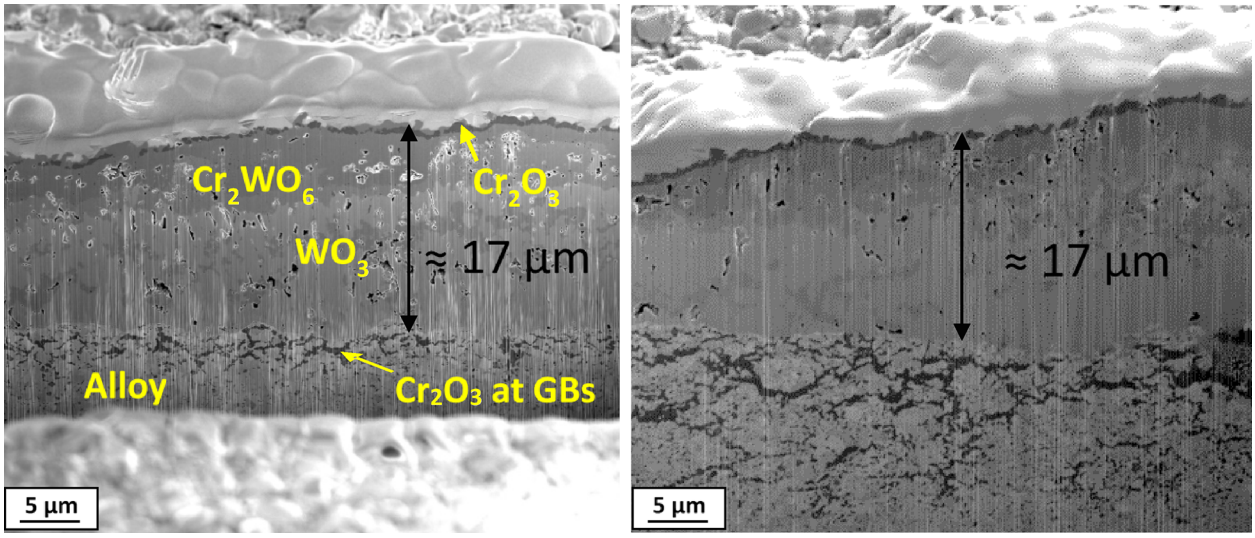

Fig. 5. Cross-section after HIP + HT of (left) W-10Cr-0.5Y and (right) W-10Cr-0.5Y-0.5Zr s after isothermal oxidation tests.

reinforcement. According to this, it becomes clear that Zr has a very positive influence on the mechanical strength of W-Cr-Y alloys, resulting in an improvement of thermal-shock resistance compared also to pure W. In future work, the mechanical properties of HTed W–10Cr–0.5Y–0.5Zr alloy will be measured.

It has to be taken into account that the materials were tested under conditions relevant for ELMs at the divertor in order to compare them with existent tests on pure W reference materials. However, self-passivating alloys are developed mainly for the blanket FW, where the load will be significantly lower. Nevertheless, in a DEMO-like device massive gas injection will be used to mitigate or avoid disruptions; this gas injection will produce photon flashes, resulting in similar loads at the blanket FW to those applied here in a single pulse. Thus, the tests presented here would simulate the load at the first wall after 1000

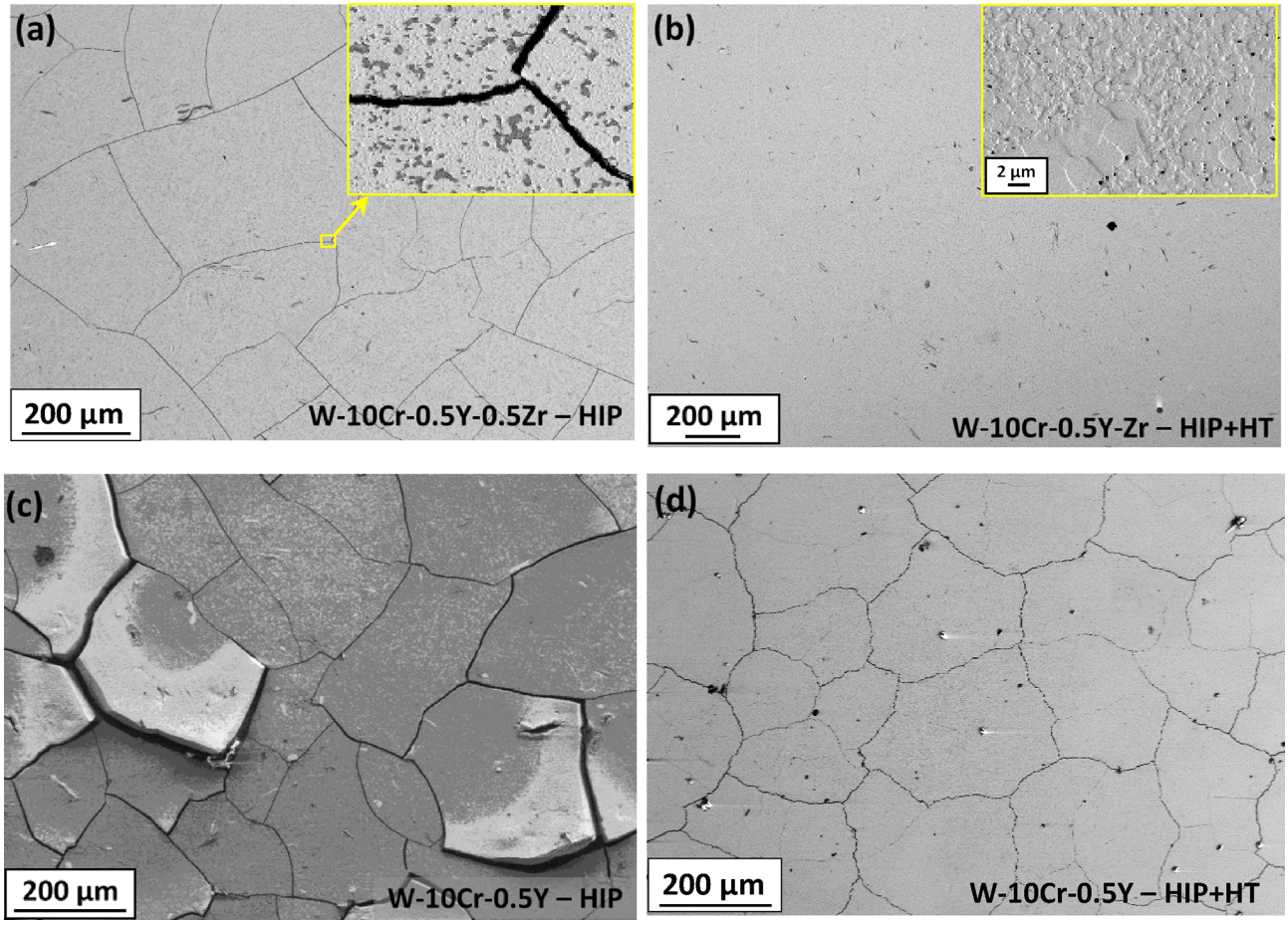

Fig. 6. Surface after loading at PSI-2 with 1000 ELM-like pulses of 0.38 GW/m^2 for 1 ms at 400 °C on (a) as-HIPed and (b) HIP + HTed W-10Cr-0.5Y-0.5Zr alloy. For comparison, surface after the same loading at JUDITH-1 on as HIPed (c) and HTed (d) W-10Cr-0.5Y alloy.

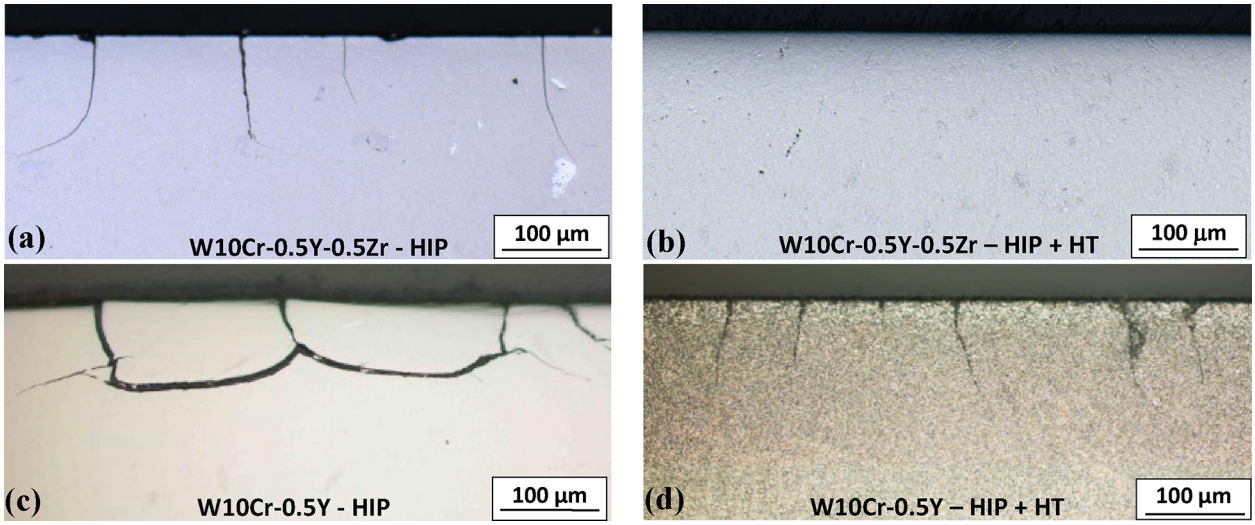

Fig. 7. Cross sections after loading at PSI-2 with 1000 ELM-like pulses of 0.38 GW/m^2 for 1 ms at 400 °C on (a) as-HIPed and (b) HIP + HTed W-10Cr-0.5Y-0.5Zr alloy. For comparison, cross sections after the same loading at JUDITH-1 on as HIPed (c) and HIP + HTed (d) W-10Cr-0.5Y alloy.

mitigated disruptions.

The Zr-containing alloys were also subjected to one pulse of 1.6 GW/m^2 for 2 ms at 400 °C at the PSI-2 facility simulating a disruption-like load. In a previous work, the samples of the reference material were exposed to 1.13 GW/m^2 during 5 ms at 400 °C at JUDITH-1. Even though the conditions are not exactly the same, the heat flux factors (72 MW/m^2·s^{½} for the Zr–containing alloy and 80 MW/m^2·s^{½} for the reference alloy) are similar for both tests and can be considered as comparable.

The surfaces of HIP + HTed W–10Cr–0.5Y-0.5Zr and reference alloys are shown in Fig. 8. Spherical pores as well as depressions and protrusions can be observed suggesting partial surface melting in both alloys. According to the W-Cr phase diagram [27] the melting temperature of the alloy is about 2750 °C. Assuming that the Zr-containing alloy has the same thermal conductivity and specific heat than the reference alloy [9], the expected temperature increase calculated according to [28] is above 6000 °C, in line with the experimental observations. Even though the samples do not exhibit catastrophic failure, it is clear that the material would not survive a disruption. Nevertheless, the HTed Zr-containing alloy would be able to withstand many mitigated disruptions without damage. This reaffirms the need for developing strategies for controlling and mitigating disruptions in DEMO.

A summary of the results obtained during ELM- and disruption-like loading is shown in Table 2.

4. Conclusions

Self- passivating bulk W-based alloys of compositions W-10Cr-0.5Zr, W-10Cr-0.5Y-0.5ZrC and W-10Cr-0.5Y-0.5Zr alloys were manufactured by MA and HIP. The W-10Cr-0.5Y-0.5Zr alloy containing both 0.5 wt% Y and Zr exhibits a high density number of NP dispersed along GBs –thus inhibiting grain growth- as well as inside the grains. Besides, screening oxidation tests reveal that the oxidation behavior of this alloy is similar to the one of the reference alloy W–10Cr-0.5Y. For alloys containing 0.5ZrC (W-10Cr-0.5Y-0.5ZrC) or 0.5Zr without Y (W-10Cr-0.5Zr) a slight Co contamination from MA was detected after the screening oxidation test. According to these results, the best system with regard to microstructure and impurity content was W-10Cr-0.5Y-0.5Zr.

Additional samples of W-10Cr-0.5Y-0.5Zr were manufactured. The as-HIPed material exhibits a nanocrystalline W-rich matrix with grains sizes below 100 nm and an extremely fine NP dispersion. During HT at 1555 °C grain growth occurs, but the matrix grain size of the Zr-containing alloy remains smaller (620 nm) than the one of the alloy

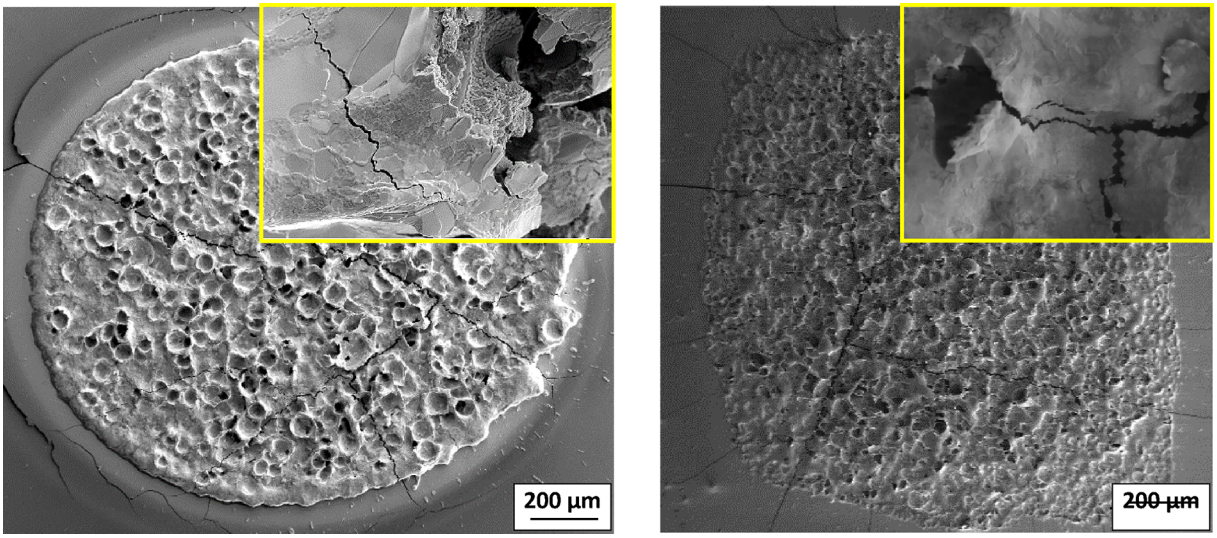

Fig. 8. Sample surface after loading at PSI-2 with one pulse of 1.6 GW/m^2 for 2 ms at 400 °C on HTed W–10Cr-0.5Y-0.5Zr alloy (left). For comparison, loading at JUDITH-1 of 1.13 GW/m^2 for 5 ms on HTed W-10Cr-0.5Y alloy (right).

Table 2
Test conditions and results of ELM- and disruption loading.

P (GW/m^2)	Base T (°C)	Pulse length (ms)	Number of pulses	Damage			
				W-10Cr-0.5Y		W-10Cr-0.5Y-0.5Zr	
				as-HIPed	HIP + HT	as-HIPed	HIP + HT
0.19	400	1	1000	No	No	No	No
0.38		1	100	Crack network, horizontal cracks, chipping	–	No	No
0.38		1	1000	Crack network, chipping	Crack network	Crack network	No
1.13		5	1	Catastrophic failure	Crack network and partial melting	–	–
1.6		2		–	–	Crack network and partial melting	Crack network and partial melting

without Zr (813 nm). Besides, in the Zr-containing alloy a NP dispersion is found both at the GBs and inside the grains. The oxygen present in the alloy is consumed by combining with the whole Y amount and part of the Zr, and it is assumed that part of the Zr combines with the C introduced during MA to form ZrC resulting in a higher strength. This has to be confirmed by TEM in future work.

Regarding oxidation, the mass gain of the Zr-containing alloy is slightly lower than the one of the reference alloy in both isothermal oxidation tests at 1000 °C for 60 h and tests under accident-like condition. However, in both alloys the total oxidized scale thickness after isothermal oxidation at 1000 °C for 60 h is nearly the same, indicating that Zr does not significantly improve (nor worse) the passivating properties compared to the reference alloy.

Under thermal shock loading consisting of 1000 ELM-like pulses, Zr-containing alloys present better resistance in comparison with the alloy without Zr, especially in the material after HT (single-phase material) where the sample does not exhibit any damage.

In view of all results, the HTed W-10Cr-0.5Y-0.5Zr system can be considered as a promising blanket FW armor material.

CRediT authorship contribution statement

Elisa Sal: Writing - original draft, Investigation. **Carmen García-Rosales:** Writing - review & editing, Supervision. **Karsten Schlueter:** Investigation. **Katja Hunger:** Investigation. **Mauricio Gago:** Investigation. **Marius Wirtz:** Investigation. **Aida Calvo:** Investigation. **Iñigo Andueza:** Resources. **Rudolf Neu:** Validation. **Gerald Pintsuk:** Validation.

Declaration of Competing Interest

The authors declare that they have no known competing financial interests or personal relationships that could have appeared to influence the work reported in this paper.

Acknowledgments

This work has been carried out within the framework of the EUROfusion Consortium and has received funding from the Euratom research and training programme 2014-2018 and 2019-2020 under grant agreement No 633053. The views and opinions expressed herein do not necessarily reflect those of the European Commission.

References

[1] D. Maisonnier et al., A Conceptual Study of Commercial Fusion Power Plants, Final Report, 2005, EFDA-RP-RE-5.0.
[2] N.P. Taylor, R. Pampin, Activation properties of tungsten as a first wall protection in fusion power plants, Fusion Eng. Des. 81 (2006) 1333–1338.
[3] D. Maisonner, I. Cook, S. Pierre, B. Lorenzo, D.P. Luigi, G. Luciano, N. Prachai, P. Aldo, DEMO and fusion power plants conceptual studies in Europe, Fusion Eng. Des. 81 (2006) 1123–1130.
[4] F. Koch, J. Brinkmann, S. Linding, T.P. Mishra, C.h. Linsmeier, Oxidation behaviour of silicon-free tungsten alloys for use as the first wall material, Phys. Scr. 014019 (2011).
[5] P. López, et al., Manufacturing of self-passivating W-Cr-Si alloys by mechanical alloying and HIP, Fusion Eng. Des. 86 (2011) 1719–1723.
[6] S. Telu, A. Patra, M. Sankaranarayana, R. Mitra, S.K. Pabi, Microstructure and cyclic oxidation behaviour of W-Cr alloys prepared by sintering of mechanically alloyed nanocrystalline powders, Int. J. Refract. Met. H. 36 (2013) 191–203.
[7] C. García-Rosales, P. López-Ruiz, S. Alvarez-Martín, A. Calvo, N. Ordás, F. Koch, J. Brinkmann, Oxidation behaviour of bulk W-Cr-Ti alloys prepared by mechanical alloying and HIPing, Fusion Eng. Des. 89 (2014) 1611–1616.
[8] J. Linke, T. Hirai, M. Roedig, L. Singheiser, Performance of plasma-facing materials under intense thermal loads in tokamaks and stellarators, Fusion Sci. Technol. 46 (2004) 142–151.
[9] A. Calvo, et al., Self-passivating tungsten alloys of the system W-Cr-Y for high temperature applications, Int. J. Refract. Met. H. 73 (2018) 29–37.
[10] A. Calvo, C. García-Rosales, N. Ordás, I. Iturriza, K. Schlueter, F. Koch, G. Pintsuk, E. Tejado, J.Y. Pastor, Self-passivating W-Cr-Y alloys: Characterization and testing, Fusion Eng. Des 124 (2017) 1118–1121.
[11] T. Wegener, A. Litnovsky, J. Binkmann, F. Koch, C.h. Linsmeier, Development of yttrium-containing self-passivating tungsten alloys for future fusion power plants, Nuclear Mater. Energy 9 (2016) 394–398.
[12] F. Klein, T. Wegener, A. Litnovsky, M. Rasinski, X.Y. Tan, J. Gonzalez-Julian, J. Schmitz, M. Bram, J.W. Coenen, C.h. Linsmeier, Oxidation resistance of bulk plasma-facing tungsten Alloys, Nuclear Mater. Energy 15 (2018) 226–231.
[13] Z.M. Xie, R. Liu, Q.F. Fang, Y. Zhou, X.P. Wang, C.S. Liu, Spark plasma sintering and mechanical properties of zirconium micro – alloyed tungsten, J. Nucl. Mater. 444 (2014) 175–180.
[14] Z.M. Xie, R. Liu, T. Zhang, Q.F. Fang, C.S. Liu, X. Liu, G.N. Luo, Achieving high strength/ductility in bulk W-Zr-Y_2O_3 alloy plate with hybrid microstructure, Materials Design 107 (2016) 144–152.
[15] Z.M. Xie, R. Liu, S. Miao, X.D. Yang, T. Zhang, Q.F. Fang, X.P. Wang, C.S. Liu, Y.Y. Lian, X. Liu, G.N. Luo, High thermal shock resistance of the hot rolled and swaged bulk W-ZrC alloys, J. Nucl. Mater. 469 (2016) 209–216.
[16] D. Jiang, L. Xue, X. Huang, T. Wang, J. Hu, Effect of Zr additions on crystal structures and mechanical properties of binary W-Zr alloys: A first- principles study, J. Mater. Res. 34 (2019) 290–300.
[17] Z.M. Xie, R. Liu, S. Miao, X.D. Yang, T. Zhang, X.P. Wang, Q.F. Fang, C.S. Liu, G.N. Luo, Y.Y. Lian, X. Liu, Extraordinary high ductility/strength of the interface designed bulk W-ZrC alloy plate at relatively low temperature, Sci. Rep. 5 (2015), https://doi.org/10.1038/srep16014.
[18] X.Y. Tan, F. Klein, A. Litnovsky, et al., Evaluation of the high temperature oxidation of W-Cr-Zr self-passivating alloys, Corros. Sci. 147 (2019) 201–211.
[19] E. Sal, C. García-Rosales, I. Iturriza, I. Andueza, Nerea Burgos, High temperature microstructural stability of self-passivating W-Cr-Y alloysfor blanket first wall application, Fusion Eng. Des. 146 (2019) 1596–1599.
[20] F. Koch, S. Köppl, H. Bolt, Self passivating W-based alloys as plasma-facing material, J. Nucl. Mater. 386–388 (2009) 572–574.
[21] M. Wirtz, A. Kreter, J. Linke, G. Th Loewenhoff, G.S. Pintsuk, I. Steudel, B. Unterberg, E. Wessel, High pulse number thermal shock tests on tungsten with steady state particle background, Phys. Scr. T170 (2017) 014066.
[22] M.W. Chase, NIST-JANAF Themochemical Tables, J. Phys. Chem. Ref. Data, Monograph 9 (1998) 1–1951.
[23] A. Calvo, C. García-Rosales, F. Koch, N. Ordás, I. Iturriza, H. Greuner, G. Pintsuk, C. Sarbu, Manufacturing and testing of self-passivating tungsten alloy of different composition, Nucl. Mater. Energy 9 (2016) 422–429.
[24] I.J. McColm, Dictionary of Ceramic Science and Engineering, second ed., Springer Science +Business Media, New York, 1994.
[25] F.J.A. den Broeder, Interface reaction and a special form of grain boundary diffusion in the Cr-W system, Acta Metall. Mater. 20 (1972) 319–332.
[26] M. Wirtz, J. Linke, T. Loewenhoff, G. Pintsuk, I. Uytdenhouwen, Thermal shock tests to qualify different tungsten grades as plasma facing material Phys, Scr. T167 (2016) 14015.
[27] W-Cr phase diagram, Bulletin of Alloy Phase Diagrams Vol. 5 No. 3 1984.
[28] H.S.J.C. Carslaw, Jaeger Conduction of Heat in Solids, second ed., Clarendon Press, Oxford, 1959.